Conference paper

Pengyu Wang* and Kazuya Kobiro*

Synthetic versatility of nanoparticles: A new, rapid, one-pot, single-step synthetic approach to spherical mesoporous (metal) oxide nanoparticles using supercritical alcohols

Abstract: A simple, rapid (10 min), one-pot, single-step method for the preparation of solid and hollow spherical porous TiO_2 nanoparticles with large surface areas (100–211 m^2/g) was developed in supercritical alcohols using carboxylic acids as organic additives. The shell thickness of the hollow TiO_2 nanoparticles (20–280 nm) was controlled by adjusting the heating rate (2.0–10.0 °C/min). The preparation of different spherical porous metal oxide nanoparticles, including CeO_2, SiO_2, TiO_2, ZrO_2, and ZnO, demonstrated the versatility of the synthetic approach. In addition, several rare earth-doped spherical mesoporous metal oxide nanoparticles, including CeO_2:Er, CeO_2:Er,Yb, ZrO_2:Er, and TiO_2:Er, which exhibit energy upconversion emission, were successfully prepared using this one-pot, single-step, supercritical methanol method. The obtained spherical mesoporous CeO_2:Er and CeO_2:Er,Yb nanoparticles emit green light upon excitation, even when irradiated with a low-power IR laser (980 nm, 10 mW) without calcination. Several other (metal) elements were also easily doped into spherical, mesoporous TiO_2 nanoparticles, such as Eu, Ce, Yb, Fe, and N, using a similar procedure. Furthermore, the spherical mesoporous TiO_2 nanoparticles were successfully applied as a new material for the transport of DNA via biolistic bombardment.

Keywords: mesoporous nanoparticles; NMS-IX; one-pot single-step synthesis; supercritical alcohols.

***Corresponding authors: Kazuya Kobiro,** School of Environmental Science and Engineering, Kochi University of Technology, 185 Miyanokuchi, Tosayamada, Kami, Kochi 782-8502, Japan, e-mail: kobiro.kazuya@kochi-tech.ac.jp; and
Pengyu Wang, School of Environmental Science and Engineering, Kochi University of Technology, 185 Miyanokuchi, Tosayamada, Kami, Kochi 782-8502, Japan, e-mail: wang.pengyu@kochi-tech.ac.jp

Article note: Paper based on a presentation at the 9th International Symposium on Novel Materials and their Synthesis (NMS-IX) and the 23rd International Symposium on Fine Chemistry and Functional Polymers (FCFP-XXIII), Shanghai, China, 17–22 October 2013.

Introduction

Recently, porous materials such as zeolites [1–3], metal organic frameworks [4–6], and metal oxides [7–10] have been intensely studied because of their large surface areas and controlled pore dimensions, and have found wide application in the fields of gas absorption, separation, condensation, drug delivery, and substrate-size-controlled catalysis [1–10]. Among them, mesoporous metal oxide (MO) nanoparticles (NPs), such as silicon dioxide (SiO_2) [10–16], titanium dioxide (TiO_2) [17–25], cerium dioxide (CeO_2) [26–28], zirconium dioxide (ZrO_2) [29–31], nickel oxide (NiO) [32–37], $LiMn_2O_4$ [38–41] and variants of these materials [42, 43], have been used as chemical catalysts, semiconductors, drug delivery vehicles, and energy storage materials. Spherical porous MO nano/microparticles with dimension-controlled morphology are particularly suited for practical applications because they possess several unique properties, such as ease of handling, effective

catalyst recovery, excellent thermal stability, a monodisperse nature, and exceptional light-harvesting properties [44–46]. These structures can be obtained using hydrothermal, sol–gel, and self-assembly methods, or a combination of these methods. However, these techniques generally require long reaction times (several hours) and complex multistep operations [1–43, 47, 48]. Recently, supercritical fluids have been applied in the synthesis of size- and morphology-controlled inorganic–organic hybrid metal and MO NPs [49–61]. All of these reported NP syntheses occur rapidly in supercritical fluids (several seconds to several minutes) [56–61]. However, a versatile synthetic method for micro/mesoporous spherical metal oxide NPs and their variants in supercritical fluids is yet to be established.

Herein, we report a simple, versatile method for the preparation of spherical micro/mesoporous (metal) oxide NPs, such as SiO_2, TiO_2, ZrO_2, CeO_2, and ZnO [18, 62]. This new category of spherical micro/mesoporous (metal) oxide NPs is referred to as micro/mesoporously architected, roundly integrated metal oxides (MARIMO) NPs, because their shape resembles that of MARIMO (*Cladophora aegagropila*) moss balls (Fig. 1) [18, 62].

Experimental

Titanium tetraisopropoxide ($Ti(O^iPr)_4$), tetraethyl orthosilicate (TEOS), cerium(III) nitrate hexahydrate ($Ce(NO_3)_3{\cdot}6H_2O$), zirconium(IV) oxynitrate dihydrate ($ZrO(NO_3)_2{\cdot}2H_2O$), zinc acetate dihydrate ($Zn(OCOCH_3{\cdot}2H_2O)$), erbium(III) acetate tetrahydrate ($Er(OCOCH_3)_3{\cdot}4H_2O$), ytterbium(III) acetate hydrate ($Yb(OCOCH_3)_3{\cdot}H_2O$), europium(III) acetate hydrate ($Eu(OCOCH_3)_3{\cdot}H_2O$), iron(III) nitrate nonahydrate ($Fe(NO_3)_3{\cdot}9H_2O$), methanol (MeOH), ethanol (EtOH), formic acid (HCOOH), phthalic acid, and benzoic acid were purchased from Wako Pure Chemical Industries Co. Ltd. and used as received.

Powder X-ray diffraction (XRD) patterns were obtained using a Rigaku SmartLab with graphite-monochromatized Cu*Ka* radiation. Transmission electron microscopy (TEM) and high-resolution transmission electron microscopy (HRTEM) images were taken using a JEOL JEM-2100F. Field emission scanning electron microscope (FESEM) images were obtained on a Hitachi S-5500. Nitrogen adsorption–desorption isotherms and Barrett–Joyner–Halenda (BJH) pore size distributions were determined using a BEL Japan INC Belsorp II, and the Brunauer–Emmett–Teller (BET) specific surface areas were obtained using a BET Shimadzu FlowSorb II 2300. Thermogravimetric (TG) analysis was carried out on a Bruker AXS 2020S, and Fourier transform infrared (FTIR) spectra were obtained using a JASCO FT/IR-4200. Dynamic light scattering (DLS) analyses were performed on a Photal FPAR-1000. Energy Dispersive X-ray spectrometry (EDX) mapping and spectral analysis were achieved using an Oxford Inca Energy TEM 250. Photoluminescence (PL) spectra were obtained using a Hitachi High-Technologies F-7000.

A metal salt (2 mmol) with or without an appropriate amount of a dopant precursor was added to a 0.5 mol/L solution of a carboxylic acid (HCOOH, phthalic acid, benzoic acid, maleic acid, or fumaric acid) in MeOH or EtOH (20 mL) with vigorous stirring.

– Synthesis of MARIMO NPs in supercritical alcohol with rapid heating: The MeOH or EtOH solution (3.5 mL) was transferred into a stainless steel (SUS) 316 batch-type reactor (10 mL volume). The reactor

Fig. 1 *C. aegagropila* moss balls.

was sealed with a screw cap equipped with a thermocouple for measurement of the inner reactor temperature and then heated for an appropriate time by placing it in a molten salt bath maintained at an appropriate temperature. Upon completion, the reaction was quenched by placing the reactor into an ice–water bath. After the reactor cooled completely, the screw cap was opened, and the crude product was sonicated in MeOH or EtOH (30 min) and centrifuged (6600 rpm, 10 °C, and 30 min), and then the upper layer was decanted. This procedure was repeated three times. The obtained powdery product was vacuum-dried at 30 °C for 24 h.

– Synthesis of MARIMO NPs in supercritical alcohols with slow heating: A gas chromatography oven was used to heat the reactor from 30 °C to an appropriate temperature at an appropriate heating rate. After completion of the reaction, the reactor was cooled at an appropriate rate or placed into an ice–water bath.The prepared powdery product was calcined in an electronic oven at 500 or 800 °C for 60 min in air if required.

Results and discussion

One-pot single-step synthesis of solid and hollow MARIMO NPs in supercritical alcohols

The simple treatment of a mixture of $Ti(O^iPr)_4$, phthalic acid, and MeOH at 300 or 400 °C for 10 min in an SUS 316 batch-type reactor followed by sonication in MeOH, decantation, and vacuum drying afforded white powdery products. In the FESEM and TEM images, the shape of the particles formed in both reactions was clearly revealed to be almost completely spherical with porous surfaces and similar to that of *C. aegagropila* moss balls (Figs. 1 and 2). Notably, the MARIMO particle sizes and primary crystalline sizes were different for the samples prepared at different reaction temperatures; the MARIMO particle size obtained at 300 °C was larger than that obtained at 400 °C. However, the primary particle size observed at 300 °C was smaller than that observed at 400 °C. DLS measurements indicated that the average sizes of the MARIMO TiO_2 NPs obtained at 300 and 400 °C were 300.5 ± 159.6 and 263.7 ± 99.3 nm (Fig. 3), respectively. These results suggest that the size of the MARIMO TiO_2 NPs size can be controlled simply by changing the reaction temperature. A lower reaction temperature yields larger, denser MARIMO NPs, while higher reaction temperatures lead to the formation of small and coarse MARIMO NPs.

Next, it was determined via powder XRD analysis that the MARIMO NPs consisted of crystallized anatase TiO_2 (JCPDS 21-1272) (Fig. 4). The observed lattice spacing of the MARIMO TiO_2 NPs as determined via HRTEM was 0.35 nm, which corresponds to that of the anatase (101) plane (Figs. 2d and h).

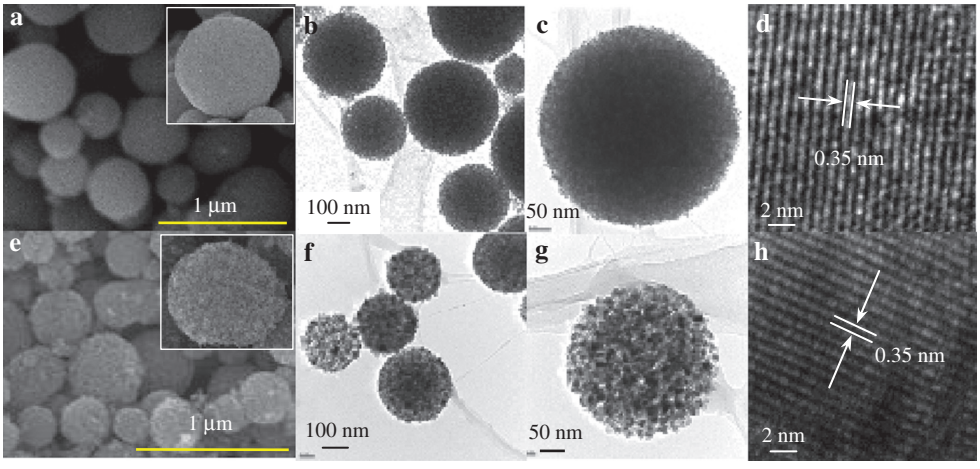

Fig. 2 FESEM (a and c) and TEM (b–d and f–h) images of MARIMO TiO_2 NPs obtained in the presence of phthalic acid in scMeOH at (a–d) 300 °C and (e–h) 400 °C.

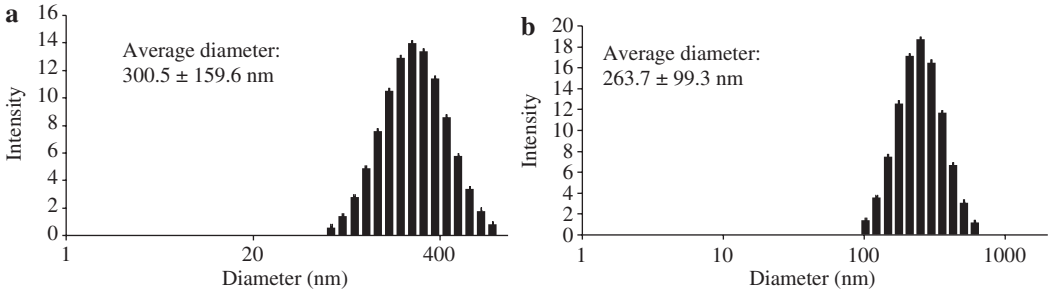

Fig. 3 DLS spectra of MARIMO TiO_2 NPs obtained in scMeOH in the presence of phthalic acid at (a) 300 °C and (b) 400 °C.

Because the surface area and pore size distribution of porous materials are very important properties, the BET surface areas, nitrogen adsorption–desorption isotherms (Fig. 5), and BJH pore size distributions of the synthesized MARIMO TiO_2 NPs were determined. Notably, the MARIMO TiO_2 NPs had BET specific surface areas (300 °C: 210.9 and 400 °C: 100.9 m^2/g) larger than that of many previously reported MARIMO TiO_2 NPs and commercially available P25 TiO_2 NPs [63, 64]. Thus, the MARIMO NPs obtained at 300 and 400 °C were classified as type IV and type II, indicating the presence of meso and macro pores, respectively (Fig. 5). The corresponding pore size distributions were 5 nm (300 °C) and 10 nm (400 °C), which were calculated using the BJH method. Calcination for anatase formation is not necessary using this method because of the inherently high temperature of supercritical MeOH (scMeOH).

FTIR reflection spectra were then obtained to determine if any organic residue remained on the surface of the MARIMO TiO_2 NPs (Fig. 6). A broad peak at 3700–3000 cm^{-1} for hydrogen-bonded O–H stretching vibrations on the surface of the TiO_2 and absorbed H_2O was observed in both FTIR spectra. The absorption peaks

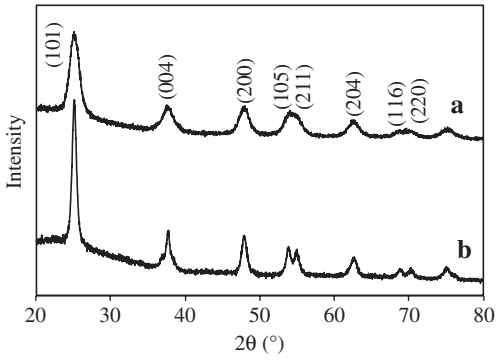

Fig. 4 XRD patterns of MARIMO TiO_2 NPs synthesized in scMeOH in the presence of phthalic acid at (a) 300 °C and (b) 400 °C.

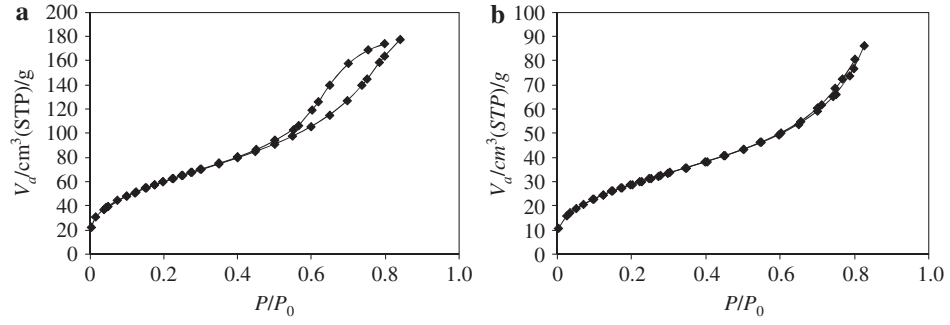

Fig. 5 Nitrogen adsorption–desorption isotherm plots for MARIMO TiO_2 NPs synthesized in scMeOH in the presence of phthalic acid at (a) 300 °C and (b) 400 °C.

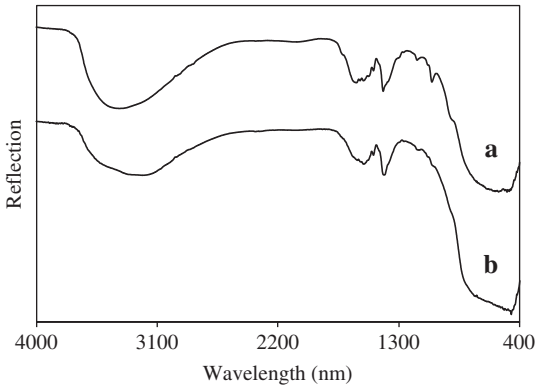

Fig. 6 FTIR reflection spectra of MARIMO TiO_2 NPs synthesized in scMeOH at (a) 300 °C and (b) 400 °C.

appearing at 1562 and 1415 cm^{-1}, also observed for the particles obtained at 300 and 400 °C, indicated that the NPs contained carboxylate (COO^-) groups (Fig. 6) [65–67]. In addition, the weight loss of the MARIMO TiO_2 NPs synthesized in the presence of phthalic acid at 300 and 400 °C was 11.5% and 12.0%, respectively, as determined via TG analysis under a N_2 gas flow, indicating that the MARIMO TiO_2 NPs contain at most ca. 12 weight% organic materials, such as phthalic acid and MeOH (Fig. 7).

Next, to elucidate the role of the organic acids in MARIMO formation, the reaction conditions were altered. First, the reaction was performed in scMeOH at 400 °C in the absence of organic acid, and it was found that the TiO_2 NPs were randomly aggregated (Fig. 8a), while the MARIMO TiO_2 NPs always formed when the acid was added (Fig. 2). Moreover, the pore sizes of the MARIMO TiO_2 NPs increased at higher concentrations of carboxylic acid (HCOOH: Figs. 9a and b; phthalic acid: Figs. 9c and d). Thus, to understand the reaction mechanism, the effect of the reaction medium was also investigated. When the reaction was performed in supercritical water (SCW) rather than scMeOH in the presence of phthalic acid at 400 °C, monodisperse,

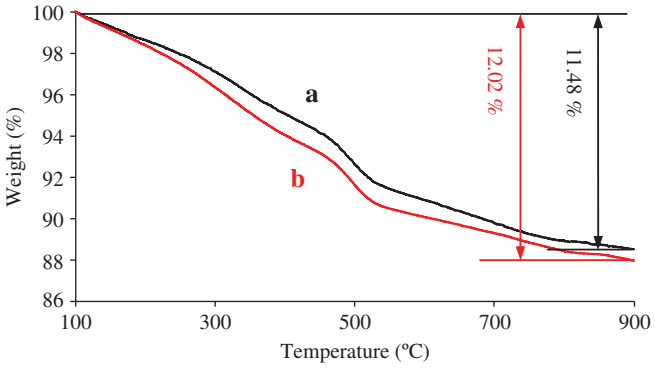

Fig. 7 TG spectra of MARIMO TiO_2 NPs synthesized in scMeOH at (a) 300 °C and (b) 400 °C.

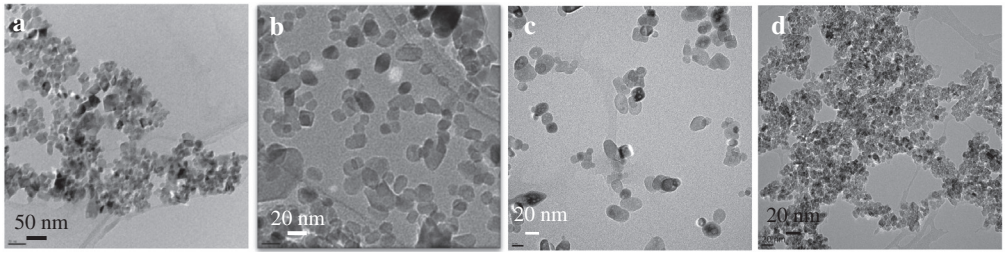

Fig. 8 TEM images of TiO_2 NPs (a) in the absence of carboxylic acid in scMeOH; (b) in the presence of phthalic acid in SCW; (c) in the presence of phthalic acid in supercritical 2-propanol; (d) in the presence of HCOOH in supercritical 2-propanol at 400 °C for 10 min.

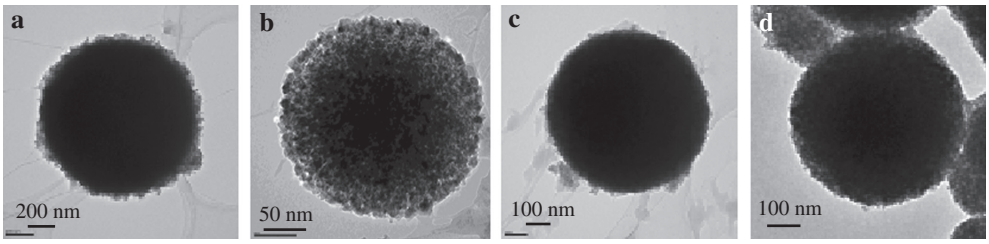

Fig. 9 TEM images of TiO_2 NPs synthesized at 300 °C for 10 min in scMeOH in the presence of different amounts of HCOOH and phthalic acid, (a) $Ti(O^iPr)_4$:HCOOH = 1:1; (b) $Ti(O^iPr)_4$:HCOOH = 1:10; (c) $Ti(O^iPr)_4$:phthalic acid = 1:1; (d) $Ti(O^iPr)_4$:phthalic acid = 1:10.

single-crystal TiO_2 NPs were obtained (Fig. 8b). Similar results were also obtained when supercritical 2-propanol was used in the presence of phthalic acid or HCOOH under similar reaction conditions (Figs. 8c and d, respectively). Thus, the combination of scMeOH and carboxylic acid is crucial for the formation of MARIMO NPs.

Next, several carboxylic acids, such as HCOOH, benzoic acid, fumaric acid, and maleic acid, were introduced to the reaction under similar reaction conditions to elucidate the effect of the organic acid on the MARIMO structure. All of the reactions afforded anatase-type TiO_2. When HCOOH or benzoic acid was used as the organic additive, a family of MARIMO TiO_2 NPs was clearly observed in the FESEM images (Figs. 10a and c). Surprisingly, an almost completely spherical hollow MARINO structure was confirmed by TEM analysis when HCOOH was used (Fig. 10d). With benzoic acid, on the other hand, a mixture of solid and hollow MARIMO NPs was obtained (Fig. 10b). Furthermore, when fumaric and maleic acid were used, several MARIMO TiO_2 aggregates were obtained under similar reaction conditions (Fig. 11). As a result, it was concluded that the added organic acid is important in the construction of the MARIMO structure.

The one-pot, single-step supercritical alcohol method was then applied to the synthesis of other MARIMO NPs, including SiO_2, ZrO_2, CeO_2, and ZnO NPs, to investigate its versatility [62]. Each of these particles was readily obtained by exposing the corresponding metal salt (TEOS, $ZrO(NO_3)_2{\cdot}2H_2O$, $Ce(NO_3)_3{\cdot}6H_2O$, and

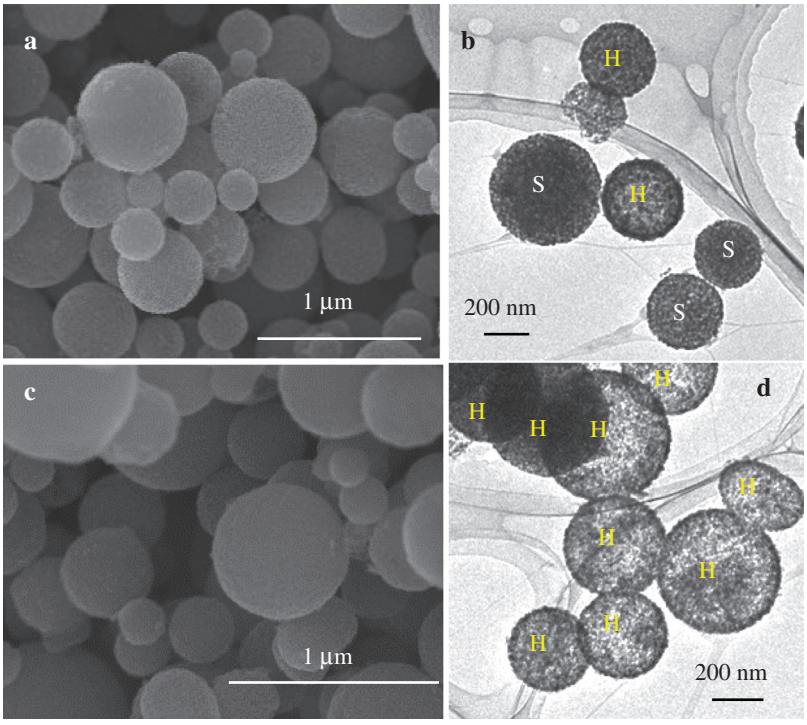

Fig. 10 FESEM (a and c) and TEM (b and d) images of MARIMO TiO_2 NPs prepared in the presence of different carboxylic acids at 400 °C for 10 min. (a) and (b) benzoic acid and (c) and (d) HCOOH. S: solid MARIMO; H: hollow MARIMO.

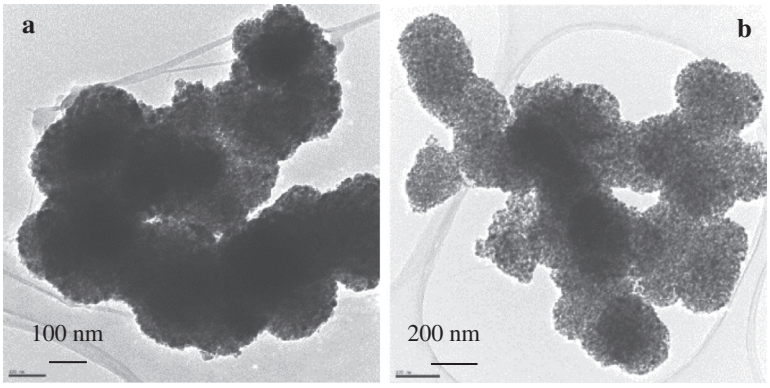

Fig. 11 TEM images of prepared mesoporous TiO_2 NPs in the presence of (a) fumaric acid and (b) maleic acid in scMeOH at 400 °C for 10 min.

$Zn(OCOCH_3)_2{\cdot}2H_2O$, respectively) to phthalic acid or HCOOH in supercritical EtOH, (scEtOH), or scMeOH (0.28 g/mL). The reaction proceeded for 10 min at 300 or 400 °C. TEM images of the SiO_2 (Figs. 12a and b), ZrO_2 (Figs. 12c and d), CeO_2 (Figs. 12e and f), and ZnO (Figs. 12g and h) NPs indicated that all of the obtained NPs possessed the MARIMO morphology. In addition, the XRD diffraction patterns of the products revealed that the crystal structure of these NPs was amorphous for SiO_2, tetragonal for ZrO_2, cubic for CeO_2, and hexagonal for ZnO NPs [62]. These results confirm the successful fabrication of MARIMO TiO_2, SiO_2, ZrO_2, and CeO_2 NPs. Thus, the simple one-pot, one-step reaction of (metal) salts in the presence of carboxylic acids in supercritical alcohols is a practical method for obtaining MARIMO NPs within a few minutes.

Synthesis of hollow MARIMO TiO_2 NPs with tunable shell thicknesses

As mentioned above, well-formed hollow MARIMO TiO_2 NPs with a very thin shell (25 ± 10 nm) were formed by rapidly heating a reaction mixture comprised of $Ti(O^iPr)_4$, HCOOH, and MeOH to 400 °C (within 30 s) (Fig. 10d) [18]. It was also found that changing the heating rate of the reaction enabled the synthesis of another new type of hollow MARIMO TiO_2 NPs with tunable shell thicknesses [62]. Slowly heating a reaction mixture of $Ti(O^iPr)_4$, phthalic acid, and MeOH from room temperature to 300 or 400 °C (ca. 5.4 °C/min) produced well-formed hollow MARIMO anatase TiO_2 NPs with thick shells (thickness 140 ± 19 and 105 ± 24 nm,

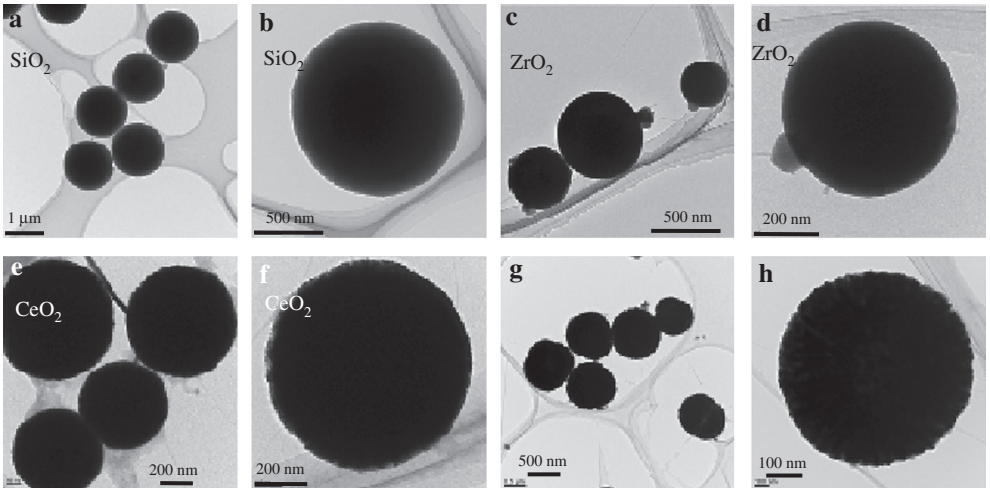

Fig. 12 TEM images of MARIMO NPs prepared in a mixture of carboxylic acid and scEtOH or scMeOH: (a and b) SiO_2, (c and d) ZrO_2, (e and f) CeO_2, and (g and h) ZnO.

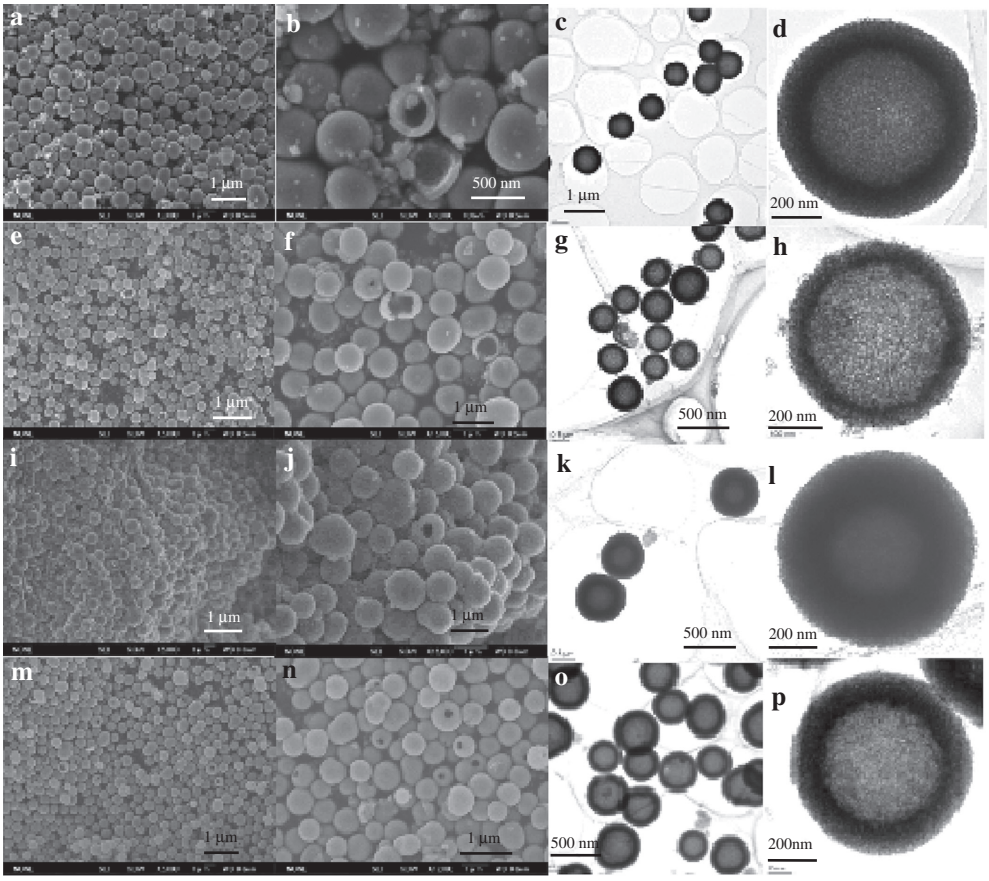

Fig. 13 TEM images of the MARIMO TiO_2 NPs prepared in the presence of phthalic acid in scMeOH under the following conditions: gradual increase in the reaction temperature from room temperature to (a, b, c, and d) 300 °C (rate of increase, 5.4 °C/min), (e, f, g, and h) 400 °C (5.4 °C/min), (i, j, k, and l) 300 °C (2 °C/min), and (m, n, o, and p) 300 °C (10 °C/min); final temperature maintained for 10 min.

respectively; 300 °C: Figs. 13a–d and Fig. 14a; 400 °C: Figs. 13e–h and 14b). The hollow structures of the NPs were directly confirmed via FESEM analysis of broken particles (Figs. 13b and f). Small primary NPs (Fig. 13d) were obtained when the solution was heated to the lower temperature (300 °C), while larger particles (Fig. 13h) were produced when the solution was heated to the higher temperature, which is consistent with the results obtained for solid MARIMO TiO_2 NPs [18]. The specific surface area of the hollow MARIMO TiO_2 NPs obtained at 300 °C after heating at 5.4 °C/min was 178 m^2/g, and these NPS contained mesopores (Fig. 15). In addition, slower heating (ca. 2 °C/min) provided hollow MARIMO anatase TiO_2 NPs with a thicker shell (281 ± 95 nm; Figs. 13i–l and 14c), while more rapid heating (ca. 10 °C/min) reduced the shell thickness to 120 ± 27 nm (Figs. 13 m–p and 14d). Thus, the thickness of the hollow MARIMO NPs is determined by the heating rate. Compared with the synthetic method using an SiO_2 microsphere template [19], this approach is much more interesting, novel, and considerably simpler, because the shell thickness and pore size of the hollow MARIMO TiO_2 NPs is controlled by merely changing the heating rate of the one-pot, single-step reaction.

Formation mechanism of solid and hollow MARIMO TiO_2 NPs

A carboxyl-group-assisted process is proposed for the formation of the solid MARIMO NPs (Scheme 1) [18, 62]. First, sterically bulky isopropoxy groups on the titanium are substituted by less-bulky methoxy groups to form primitive titanium alkoxide oligomers via transesterification at high temperature in the presence

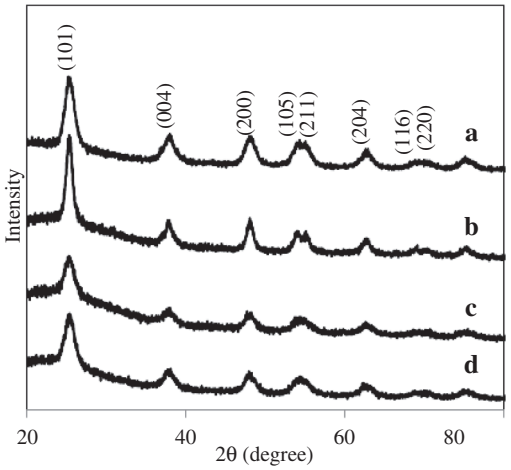

Fig. 14 Powder XRD patterns of the MARIMO TiO_2 NPs prepared in a mixture of phthalic acid in scMeOH under the following conditions: gradual increase in the reaction temperature from room temperature to (a) 300 °C (rate of increase, 5.4 °C/min), (b) 400 °C (5.4 °C/min), (c) 300 °C (2 °C/min), and (d) 300 °C (10 °C/min); final temperature maintained for 10 min.

of a carboxylic acid in MeOH [68]. As the reaction mixture is heated further, the esterification of the acids with MeOH leads to the generation of water. The titanium alkoxide oligomers bearing carboxylic acids then react with water to form TiO_2 crystals [48]. Under these conditions, the carboxyl groups connect with some of the primitive particles via surface interactions. The carboxyl groups can be –COOH, $–COO^-$, or $–COOCH_3$. Among these carboxyl groups, –COOH groups can be from the unreacted carboxylic acid; $–COOCH_3$ groups can be provided in the esterification reaction of carboxylic acid and MeOH; $–COO^-$ groups can be afforded by carboxylic acid in the presence of H_2O. Then decomposition of the carboxylic acids leads to the evolution of gaseous products such as CO_2. These processes occur rapidly during rapid heating (within 30 s), with consequent expansion of the spherical NPs to yield either solid or thin-shelled hollow MARIMO NPs (Scheme 1, rapid heating). In addition, the primary particle size obtained at 300 °C was smaller and denser than that obtained at 400 °C. These results can be explained by the Ostwald ripening. Namely, small primary particles can be dissolved and grow on the large primary particles at a higher temperature. Therefore the MARIMO TiO_2 nanoparticles become small and sparse while the pore size becomes large at high temperature. On the other hand, hollow thick-shelled MARIMO NPs are formed at a slow heating rate via the Ostwald ripening effect (Scheme 1, slow heating) [69–76]. Because amorphous MARIMO TiO_2 formation was confirmed at low reaction temperatures (200 °C) and slower heating rates increased the shell thickness of the NPs, it can be inferred that the amorphous TiO_2 initially generated at low temperatures becomes crystalline as the temperature rises, concomitant with enhancement of the Ostwald ripening effect. Thus, poorly formed crystals are lost, resulting in larger and more complete single crystals with the thick-shelled hollow MARIMO morphology.

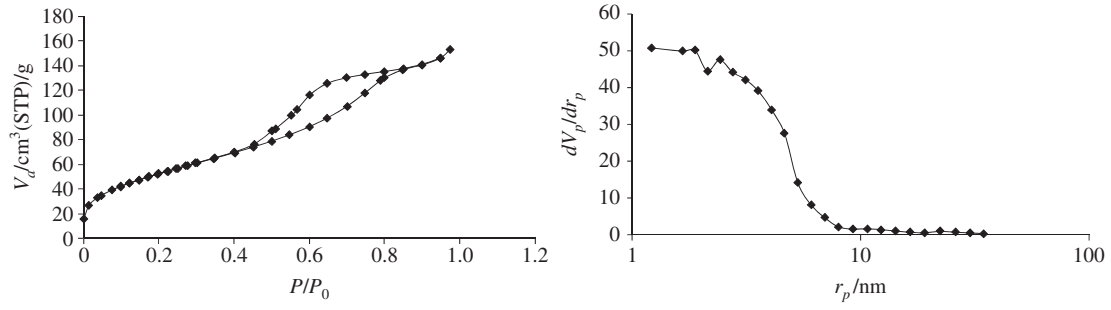

Fig. 15 Nitrogen adsorption–desorption isotherm and BJH pore size distribution plots for MARIMO TiO_2 NPs prepared at 300 °C for 10 min in the presence of phthalic acid (slow heating: 5.4 °C/min).

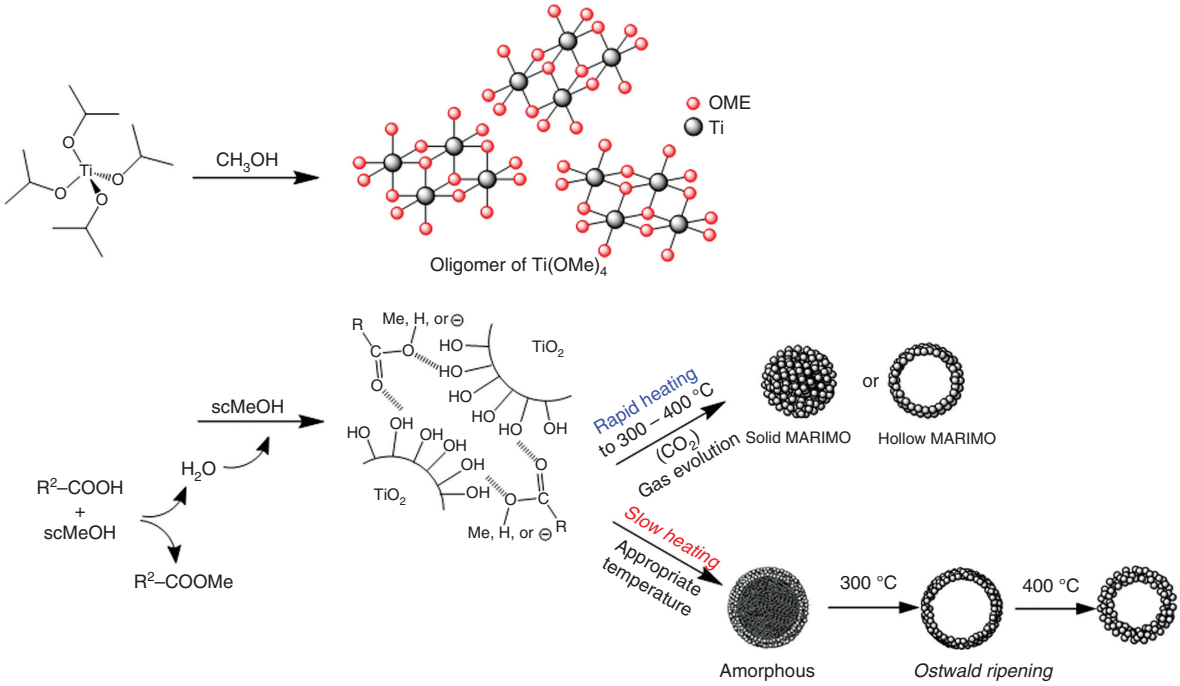

Scheme 1 Plausible mechanism for the formation of solid and hollow MARIMO TiO_2 NPs in scMeOH.

One-pot single-step synthesis of element-doped MARIMO NPs in supercritical alcohols

This simple method can also be used for the preparation of upconversion (UC) fluorescent MARIMO NPs via the introduction of appropriate rare earth (RE) elements, such as Er^{3+}, Eu^{3+}, Yb^{3+}, and Ce^{3+}, as dopants into the reaction mixture [77]. It is well known that a smaller phonon energy leads to smaller multiphonon relaxation rates, which improves the fluorescence intensity in UC materials [78]. To achieve a lower phonon energy and higher emission intensity, a host material with a high atomic weight, such as CeO_2, and a dopant that emits green light under IR laser irradiation, such as Er^{3+}, are typically used. Thus Er^{3+} doped mesoporous spherical CeO_2 (CeO_2:Er) NPs were synthesized by heating a homogeneous solution of $Ce(NO_3)_3{\cdot}6H_2O$, $Er(OCOCH_3)_3{\cdot}4H_2O$, and HCOOH (molar ratio 10:1:50) in scMeOH (0.28 g/mL) at 300 °C for 10 min. EDX mapping images of the obtained CeO_2:Er (10:1) [79] MARIMO NPs indicated that 3.2 mol% Er was dispersed homogeneously throughout the MARIMO CeO_2 NPs (Figs. 16a and 17a) [80]. In addition, the XRD pattern for CeO_2:Er (10:1) was identical to that of the prototype CeO_2 NPs. Given these results, it can be concluded that the Er atoms were embedded in the crystal lattice. However, the NPs never fluoresced under excitation using a low-intensity IR laser (980 nm, 10 mW), even after calcination. The likely cause of this phenomenon is concentration quenching. Therefore, the content of Er in the CeO_2:Er MARIMO NPs was reduced; a homogeneous solution of $Ce(NO_3)_3{\cdot}6H_2O$, $Er(OCOCH_3)_3{\cdot}4H_2O$, and HCOOH (100:1:500) was heated in scMeOH under similar conditions. This process yielded CeO_2:Er (100:1) particles that appeared to be MARIMO NPs (Fig. 16b). In addition, the morphology and cubic crystal structure of the MARIMO NPs were unaltered by calcination (TEM: Figs. 16b and c; XRD: Figs. 17b and c). As can be seen in Fig. 18a, the absorption band for the O–H stretching vibration in the FTIR spectrum decreased after calcination, indicating that the dehydration of particles occurred. Therefore, proton evacuation may take place as a result of ion diffusion during sintering. The BET specific surface area of the calcined NPs (800 °C) was 15.3 m^2/g, and the pores were 2–15 nm mesopores (Fig. 19a and b).

Importantly, the obtained particles emitted green light under low-intensity IR laser irradiation (980 nm, 10 mW), even without calcination (Fig. 20a). Two emission bands at approximately 550 nm (green) and 680 nm (red) were observed in the PL spectrum of the irradiated NPs that are attributed to the $^2H_{11/2}$,$^4S_{3/2} \rightarrow {}^4I_{15/2}$

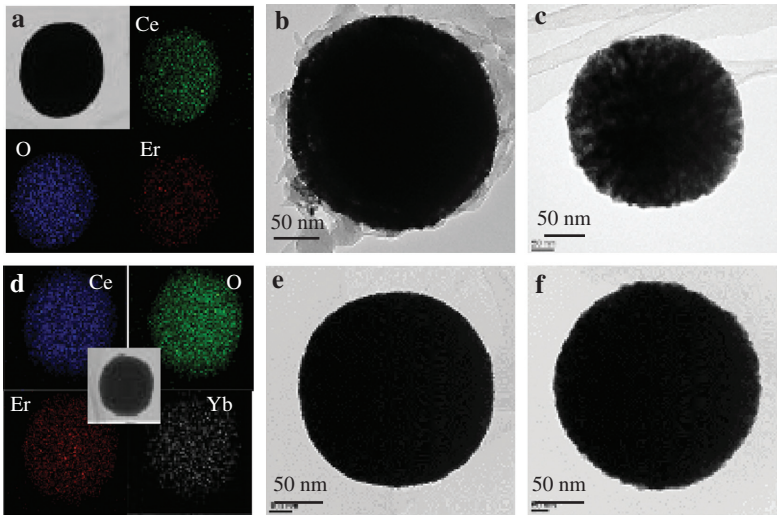

Fig. 16 TEM and EDX mapping images of RE-doped MARIMO NPs. (a) CeO_2:Er (10:1) before calcination; (b) CeO_2:Er (100:1) before calcination; (c) CeO_2:Er (100:1) after calcination; (d) CeO_2:Er,Yb (10:1:1) before calcination; (e) CeO_2:Er,Yb (100:1:1) before calcination, and (f) CeO_2:Er,Yb (100:1:1) after calcination.

and $^4F_{9/2} \rightarrow {}^4I_{15/2}$ emissions of Er^{3+}, respectively (Fig. 21a). As expected, the intensity of both peaks increased following calcination at 500 °C for 60 min, and further improved when the NPs were calcined at 800 °C for 60 min (Fig. 20b and Figs. 21b and c, respectively). In addition, the presence of organic residues on the MARIMO NPs was confirmed via FTIR analysis (Fig. 18). Peaks for the stretching vibrations of hydrogen-bonded O–H groups on the surface of the primary NPs (3700–3000 cm^{-1}) and absorptions for COO^- groups (1650–1550 and 1410 cm^{-1}) disappeared after calcination at 500 and 800 °C (Figs. 18b and c, respectively). In addition, the weight of the NPs decreased by 5% after calcination at 800 °C for 60 min, suggesting the removal of organic residues and water from the surface of the primary MARIMO NPs.

Next, to further explore the versatility of the one-pot, one-step synthetic procedure, the preparation of Er, Yb co-doped nanoparticles was attempted [81]. Yb co-doped CeO_2:Er MARIMO NPs, CeO_2:Er,Yb (100:1:1), were

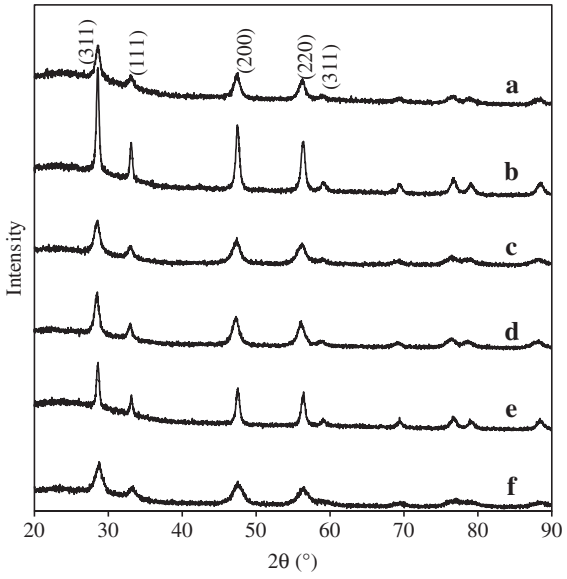

Fig. 17 XRD patterns of the RE-doped MARIMO NPs. (a) CeO_2:Er (10:1) before calcination; (b) CeO_2:Er (100:1) before calcination; (c) CeO_2:Er (100:1) after calcination; (d) CeO_2:Er,Yb (10:1:1) before calcination; (e) CeO_2:Er,Yb (100:1:1) before calcination; and (f) CeO_2:Er,Yb (100:1:1) after calcination.

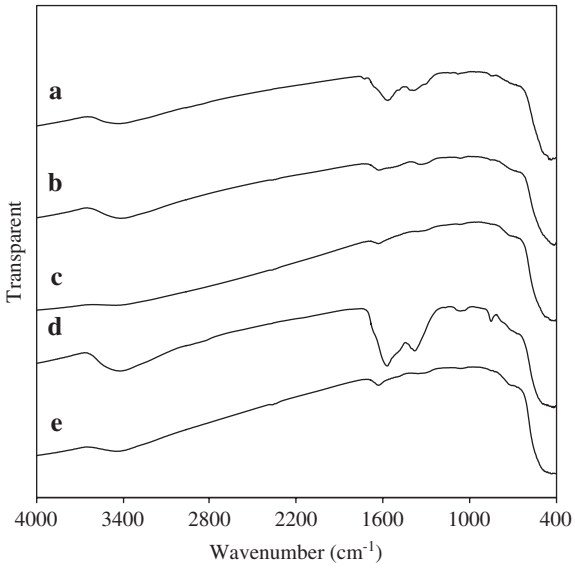

Fig. 18 FTIR spectra of CeO_2:Er (100:1) and CeO_2:Er,Yb (100:1:1) MARIMO NPs prepared in scMeOH in the presence of HCOOH. Reaction conditions: 10 min at 300 °C in MeOH with a density of 0.28 g/mL. (a) CeO_2:Er (100:1) without calcination; (b) CeO_2:Er (100:1) with calcination at 500 °C for 60 min in air; (c) CeO_2:Er (100:1) with calcination at 800 °C for 60 min in air; (d) CeO_2:Er,Yb (100:1:1) without calcination; and (e) CeO_2:Er,Yb (100:1:1) with calcination at 800 °C for 60 min in air.

synthesized by heating a homogeneous solution of $Ce(NO_3)_3{\cdot}6H_2O$, $Er(OCOCH_3)_3{\cdot}4H_2O$, $Yb(OCOCH_3)_3{\cdot}nH_2O$, and HCOOH (100:1:1:500) in scMeOH [79] (Figs. 16e and f). EDX mapping of the CeO_2:Er,Yb (10:1:1) particles [79, 80] revealed the homogeneous distribution of 3.0 mol% Er and 3.1 mol% Yb throughout the MARIMO NPs (Fig. 16d). XRD measurements indicated a cubic crystal structure, which was retained after calcination (Figs. 17d, e, and f). The pores of the calcined NPs were classified as mesopores with diameters of 2–15 nm, and the BET specific surface area was 16.0 m^2/g (Figs. 19c and d). Calcination removed all of the organic residues (Figs. 18d and e); however, even for the noncalcined samples, a strong green emission was observable by the naked eye under low-intensity IR laser irradiation (980 nm; 10 mW), (Fig. 20c). In addition, as anticipated,

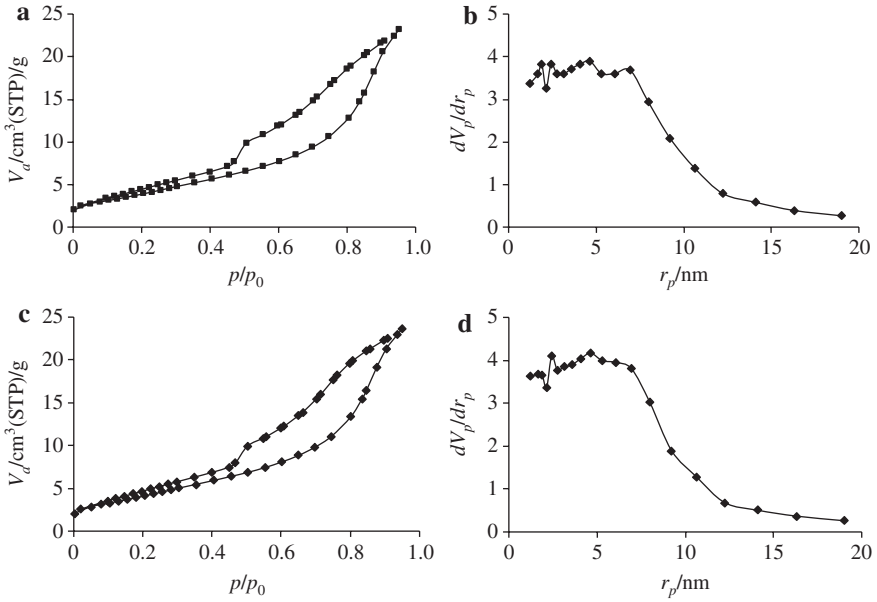

Fig. 19 Nitrogen adsorption–desorption isotherm and BJH pore size distribution plots for MARIMO RE-doped UC NPs prepared in scMeOH after calcination at 800 °C for 60 min. (a and b) CeO_2:Er (100:1) and (c and d) CeO_2:Er,Yb (100:1:1).

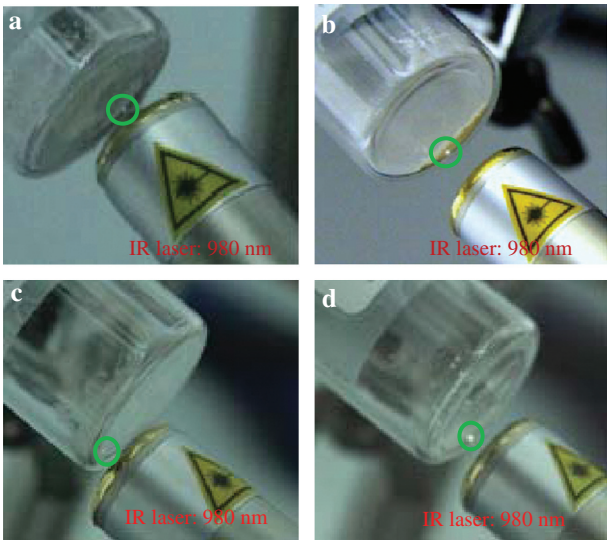

Fig. 20 Green emission of MARIMO NPs. CeO_2:Er (100:1): (a) before and (b) after calcination at 800 °C for 60 min in air; CeO_2:Er,Yb (100:1:1): (c) before and (d) after calcination at 800 °C for 60 min in air.

the emission intensity was enhanced by calcination (Fig. 20d). Two emission bands were also observed near 550 and 680 nm in the PL spectra of the NPs (Figs. 21d and e), and the intensity of the red emission was greater than that in the green region due to the efficient energy transfer from the Yb co-dopant to the Er luminescence center [81]. These results confirmed that Yb co-doped CeO_2:Er MARIMO NPs with efficient UC emission were successfully prepared via the one-pot, single-step reaction in scMeOH. To the best of our knowledge, previously reported NPs always required calcination to achieve emission [82–87]. However, in the present case, calcination is not necessary for UC emission, even under low power IR laser irradiation (980 nm, 10 mW),

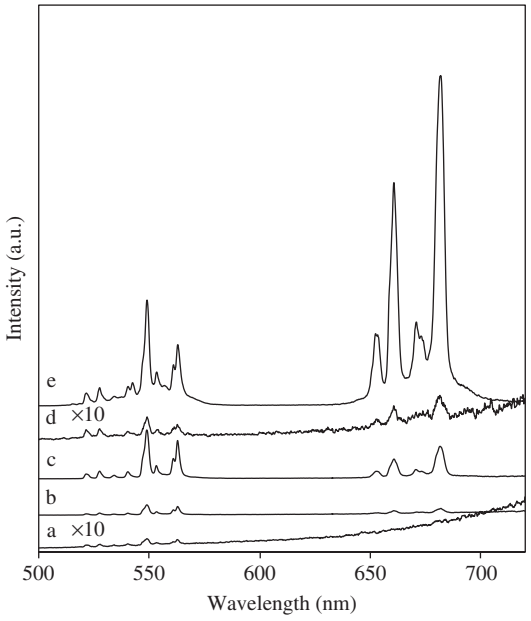

Fig. 21 PL spectra (under IR irradiation at 980 nm) of CeO_2:Er and CeO_2:Er,Yb MARIMO NPs prepared from a mixture of scMeOH and formic acid. Reaction conditions: 10 min at 300 °C in MeOH with a density of 0.28 g/mL. (a) CeO_2:Er (100:1) without calcination; (b) CeO_2:Er (100:1) with calcination at 500 °C for 60 min; (c) CeO_2:Er (100:1) with calcination at 800 °C for 60 min; (d) CeO_2:Er,Yb (100:1:1) without calcination; and (e) CeO_2:Er,Yb (100:1:1) with calcination at 800 °C for 60 min.

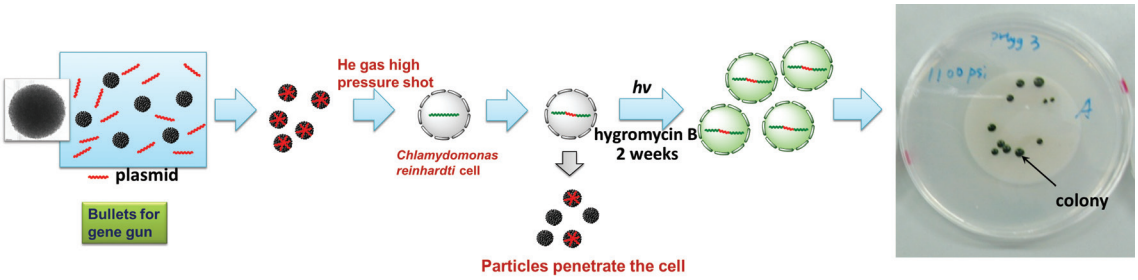

Fig. 22 DNA transport via biolistic bombardment using MARIMO TiO_2 NPs as bullets for the gene gun.

which could be because of the unique light harvesting properties of the mesoporous structure of the MARIMO NPs [46, 88]. When mesoporous NPs are irradiated, they allow the light to scatter to the interior, leading to the formation of multiple reflections between the primary particles. Therefore, the pores can provide a light harvesting effect that results in more efficient light absorption compared with that observed for normal NPs [46, 88]. Furthermore, the mesoporous structure of the MARIMO NPs with UC ability may be very suitable for the delivery of drugs and sensitizers or as agents for photodynamic therapy.

The unique one-pot, single-step simultaneous doping approach is also applicable to other MARIMO NPs. The process has been used to prepare ZrO_2:Er, TiO_2:Er, TiO_2:Eu (10:1), TiO_2:Ce (10:1), TiO_2:Yb (10:1), and TiO_2:Fe (10:1) MARIMO NPs using the scMeOH method [77]. Therefore, it has been clearly demonstrated that this synthetic approach is highly versatile for the preparation of MARIMO NPs doped with a wide range of elements.

MARIMO TiO_2 NPs as a new biolistic bombardment agent

Finally, the MARIMO TiO_2 NPs were successfully applied as a new material for transporting DNA via biolistic bombardment [62, 89]. The gold and tungsten NPs currently used for biolistic bombardment are classified as nanoaggregates, with average aggregation sizes of several hundred nanometers. The MARIMO TiO_2 NPs prepared in this study have a size-controlled, spherical structure with numerous mesopores that can readily admit plasmids. The MARIMO TiO_2 NPs shown in Fig. 1a were mixed with a supercoiled pHyg3 plasmid carrying the hygromycin resistance gene aphVII. The particles were then shot into *Chlamydomonas reinhardtii* cells using high pressure He gas (7.6 MPa). After two weeks, colonies appeared on hygromycin-infused agar plates, confirming that the novel MARIMO TiO_2 NPs successfully transported the DNA via biolistic bombardment (Fig. 22). Thus, despite their reduced density, the MARIMO TiO_2 NPs delivered the DNA; therefore, they should be considered as an alternative to the heavy, expensive gold and tungsten NPs currently used for DNA transport.

Conclusions

MARIMO NPs with large surface areas, such as TiO_2, SiO_2, ZrO_2, CeO_2, and ZnO, were successfully synthesized via a simple, rapid, one-pot, one-step process in supercritical alcohols with carboxylic acids (phthalic acid and HCOOH) as organic additives. In addition, a new type of hollow TiO_2 NPs was obtained when the reaction mixture was heated slowly, and notably, the thickness of the shells of these NPs could be controlled by adjusting the heating rate. Furthermore, the synthetic versatility of the one-pot, one-step method for the preparation of MARIMO NPs was demonstrated by synthesizing a series of solid and hollow MARIMO NPs and RE element-doped MARIMO UC fluorescent NPs, such as CeO_2:Er, CeO_2:Er,Yb, ZrO_2:Er, and TiO_2:Er, that also had large surface areas. Clear green emission was confirmed for these NPs without calcination, even under weak IR laser irradiation (980 nm, 10 mW). Strong fluorescence intensity was achieved not only for calcined CeO_2:Er NPs but also for CeO_2:Er,Yb MARIMO NPs. Finally, the synthesized MARIMO TiO_2 NPs were successfully applied to DNA transport via biolistic bombardment.

The prepared solid and hollow MARIMO NPs reported herein have several excellent properties, such as a spherical porous structure, narrow average size distribution, and large surface area. Therefore, they can be used as photocatalysts, photosemiconductors, and catalyst supports, for drug storage/controlled release and DNA transport, as a white pigment in low-reflection, transparent, and heat-insulation paints. In addition, RE-doped MARIMO NPs capable of UC stable emission may be used as cell markers for photodynamic therapy or as luminescence materials.

Acknowledgments: The authors gratefully acknowledge Mr. Masao Yamashita and Dr. Tsutomu Nakanishi of Kagawa Industry Support Foundation for the synthesis of the hollow MARIMO TiO_2 NPs. The authors also extend their sincere thanks to Prof. Tomoya Konishi of Anan National College of Technology for completing the FTIR analyses and Prof. Hiromichi Aono of Ehime University for obtaining the BET and nitrogen adsorption–desorption isotherm spectra. The authors also thank Prof. Nagatoshi Nishiwaki and Dr. Noriko Nitta of Kochi University of Technology for their fruitful discussions and Mr. Tetsuo Nagayama, Mr. Masato Sato, and Ms. Hiroko Ishikawa of the social cooperation division of Kochi University of Technology for their support. This work was partially supported by the Creation of New Business and Industry program through the Kochi Prefectural Industry-Academia-Government Collaboration Research Promotion Operation.

References

[1] H. Chen, J. Wydra, H. Zhang, P. -S. Lee, Z. Wang, W. Fan, M. Tsapatsis. *J. Am. Chem. Soc.* **133**, 12390 (2011).
[2] Q. Meng, D. C. Doetschman, A. K. Rizos, M. -H. Lee, J. T. Schulte, A. Spyros, C. W. Kanyi. *Environ. Sci. Technol.* **45**, 3000 (2011).
[3] J. Zhao, J. Zhou, Y. Chen, Q. He, M. Ruan, L. Guo, J. Shi, H. Chen. *J. Mater. Chem.* **19**, 7614 (2009).
[4] S. Xiang, Y. He, Z. Zhang, H. Wu, W. Zhou, R. Krishna, B. Chen. *Nat. Commun.* **3**, 954 (2012).
[5] N. Stock, S. Biswas. *Chem. Rev.* **112**, 933 (2012).
[6] M. Yoon, R. Srirambalaji, K. Kim. *Chem. Rev.* **112**, 1196 (2012).
[7] X. Sun, Y. Shi, P. Zhang, C. Zheng, X. Zheng, F. Zhang, Y. Zhang, N. Guan, D. Zhao, G. D. Stucky. *J. Am. Chem. Soc.* **133**, 14542 (2011).
[8] W. Cai, J. Yu, C. Anand, A. Vinu, M. Jaroniec. *Chem. Mater.* **23**, 1147 (2011).
[9] N. C. Strandwitz, G. D. Stucky. *Chem. Mater.* **21**, 4577 (2009).
[10] X. Liang, M. Yu, J. Li, Y. -B. Jiang, A. W. Weimer. *Chem. Commun.* 7140 (2009).
[11] F. Tang, L. Li, D. Chen. *Adv. Mater.* **24**, 1504 (2012).
[12] Y. L. Choi, J. H. Lee, J. Jaworski, J. H. Jung. *J. Mater. Chem.* **22**, 9455 (2012).
[13] P. Yang, S. Gai, J. Lin. *Chem. Soc. Rev.* **41**, 3679 (2012).
[14] N. Niu, F. He, P. Ma, S. Gai, G. Yang, F. Qu, Y. Wang, J. Xu, P. Yang. *ACS Appl. Mater. Interfaces* **6**, 3250 (2014).
[15] X. Li, Q. He, J. Shi. *ACS Nano* **8**, 1309 (2014).
[16] R. Qian, L. Ding, H. Ju. *J. Am. Chem. Soc.* **135**, 13282 (2013).
[17] S. B. Lee, H. L. Kim, H. -J. Jeong, S. T. Lim, M. -H. Sohn, D. W. Kim. *Angew. Chem. Int. Ed.* **52**, 10549 (2013).
[18] P. Wang, K. Kobiro. *Chem. Lett.* **41**, 264 (2012).
[19] J. B. Joo, Q. Zhang, I. Lee, M. Dahl, F. Zaera, Y. Yin. *Adv. Funct. Mater.* **22**, 166 (2012).
[20] M. P. Hong, J. Y. Kim, K. Vemula, H. S. Kim, K. B. Yoon. *Chem. Commun.* **48**, 4250 (2012).
[21] Z. Sun, J. H. Kim, Y. Zhao, F. Bijarbooneh, V. Malgras, Y. Lee, Y. -M. Kang, S. X. Dou. *J. Am. Chem. Soc.* **133**, 19314 (2011).
[22] L. J. Fu, L. C. Yang, Y. Shi, B. Wang, Y. P. Wu. *Micro. Meso. Mater.* **117**, 515 (2009).
[23] M. Faisal, A. A. Ismail, F. A. Harraz, H. Bouzid, S. A. Al-Sayari, A. Al-Hajry. *Chem. Engin. J.* **243**, 509 (2014).
[24] Q. Wu, W. Li, D. Wang, S. Liu. *Appl. Surf. Sci.* **299**, 35 (2014).
[25] M. Xu, P. Ruan, H. Xie, A. Yu, X. Zhou. *ACS Sustainable Chem. Eng.* DOI: 10.1021/sc4005586 (2014).
[26] J. Wei, Z. Yang, Y. Yang. *CrystEngComm* **13**, 2418 (2011).
[27] Z. Yang, J. Wei, H. Yang, L. Liu, H. Liang, Y. Yang. *Eur. J. Inorg. Chem.* **2010**, 3354 (2010).
[28] T. Brezesinski, J. Wang, R. Senter, K. Brezesinski, B. Dunn, S. H. Tolber. *ACS Nano* **4**, 967 (2010).
[29] Y. Chen, S. K. Lunsford, Y. Song, H. Ju, P. Falaras, V. Li-kodimos, A. G. Kontos, D. D. Dionysiou. *Chem. Engin. J.* **170**, 518 (2011).
[30] A. Mondal, A. Zachariah, P. Nayak, B. B. Nayak. *J. Am. Ceram. Soc.* **93**, 387 (2010).
[31] A. M. Hussein, R. V. Shende. *Int. J. Hydrogen Energ.* **39**, 5557 (2014).
[32] B. Wang, J. L. Cheng, Y. P. Wu, D. Wang, D. N. He. *Electrochem. Commun.* **23**, 5 (2012).

[33] Z. bai, Z. Ju, C. Guo, Y. Qian, B. Tang, S. Xiong. *Nanoscale* **6**, 3268 (2014).
[34] M. A. Behnajady, S. Bimeghdar. *Chem. Engin. J.* **239**, 105 (2014).
[35] K. Xu, R. Zou, W. Li, Q. Liu, T. Wang, J. Yang, Z. Chen, J. Hu. *New J. Chem.* **37**, 4031 (2013).
[36] M. Khairy, S. A. El-Safty. *RSC Adv.* **3**, 23801 (2013).
[37] A. Caballero, L. Hernan, 'J. Morales. *Energy Fuels* **27**, 5545 (2013).
[38] W. Tang, Y. Hou, F. Wang, L. Liu, Y. Wu, K. Zhu. *Nano Lett.* **13**, 2036 (2013).
[39] B. -M. Hwang, S. -J. Kim, Y. -W. Lee, B. Han, S. -B. Kim, W. -S. Kim, K. -W. Park. *Int. J. Electrochem. Sci.* **8**, 9449 (2013).
[40] Y. Wu, Z. Wen, H. Feng, J. Li. *Small* **8**, 858 (2012).
[41] J. M. Kim, G. Lee, B. H. Kim, Y. S. Huh, G. -W. Lee, H. J. Kim. *Ultrason. Sonochem.* **19**, 627 (2012).
[42] X. Lai, J. Li, B. A. Korgel, Z. Dong, Z. Li, F. Su, J. Du, D. Wang. *Angew. Chem. Int. Edit.* **50**, 2738 (2011).
[43] W. Li, Q. Yue, Y. Deng, D. Zhao. *Adv. Mater.* **25**, 5129 (2013).
[44] S. Liu, J. Yu, M. Jaroniec. *J. Am. Chem. Soc.* **132**, 11914 (2010).
[45] X. Hu, G. Li, J.C. Yu. *Langmuir* **26**, 3031 (2009).
[46] J. H. Pan, X. Zhang, A. J. Du, D. D. Sun, J. O. Leckie. *J. Am. Chem. Soc.* **130**, 11256 (2008).
[47] A. A. Ismail, D. W. Bahnemann. *J. Mater. Chem.* **21**, 11686 (2011).
[48] X. Chen, S. S. Mao. *Chem. Rev.* **107**, 2891(2007).
[49] S. K. Pahari, T. Adschiri, A. B. Panda. *J. Mater. Chem.* **21**, 10377 (2011).
[50] A. A. Vostrikov, O. N. Fedyaeva, A. V. Shishkin, M. Ya. Sokol. *J. Supercrit. Fluid.* **48**, 154 (2009).
[51] A. A. Vostrikov, O. N. Fedyaeva, A. V. Shishkin, M. Ya. Sokol. *J. Supercrit. Fluid.* **48**, 161 (2009).
[52] B. Veriansyah, J. -D. Kim, B. K. Min, Y. H. Shin, Y. -W. Lee, J. Kim. *J. Supercrit. Fluid.* **52**, 76 (2010).
[53] J. Zhang, S. Ohara, M. Umetsu, T. Naka, Y. Hatakeyama, T. Adschiri. *Adv. Mater.* **19**, 203 (2007).
[54] T. Arita, H. Hitaka, K. Minami, T. Naka, T. Adschiri. *Chem. Lett.* **40**, 588 (2011).
[55] T. Togashi, T. Naka, S. Asahina, K. Sato, S. Takami, T. Adschiri. *Dalton Trans.* **40**, 1073 (2011).
[56] T. Adschiri, Y. -W. Lee, M. Goto, S. Takami. *Green Chem.* **13**, 1380 (2011).
[57] F. Cansell, C. Aymonier. *J. Supercrit. Fluid.* **47**, 508 (2009).
[58] K. Byrappa, S. Ohara, T. Adschiri. *Adv. Drug Delivery Rev.* **60**, 299 (2008).
[59] T. Adschiri. *Chem. Lett.* **36**, 1188 (2007).
[60] E. Reverchon, R. Adami. *J. Supercrit. Fluid.* **37**, 1 (2006).
[61] C. Aymonier, A. Loppinet-Serani, H. Reverón, Y. Garrabos, F. Cansell. *J. Supercrit. Fluid.* **38**, 242 (2006).
[62] P. Wang, K. Ueno, H. Takigawa, K. Kobiro. *J. Supercrit. Fluids* **78**, 124 (2013).
[63] D. Chen, F. Huang, Y. -B. Cheng, R. A. Caruso. *Adv. Mater.* **21**, 2206 (2009).
[64] W. Zhang, R. Zhu, L. Ke, X. Liu, B. Liu, S. Ramakrishna. *Small* **6**, 2176 (2010).
[65] Z. Zhang, X. Zhong, S. Liu, D. Li, M. Han. *Angew. Chem., Int. Ed.* **44**, 3466 (2005).
[66] P. D. Cozzoli, A. Kornowski, H. Weller. *J. Am. Chem. Soc.* **125**, 14539 (2003).
[67] V. Tantishaiyakul, N. Phadoongsombut, W. Wongpuwarak, J. Thungtiwachgul, D. Faroongsarng, K. Wiwattanawongsa, Y. Rojanasakul. *Int. J. Pharm.* **283**, 111 (2004).
[68] D. A. Wright, D. A. Williams. *Acta Crystallogr., Sect. B: Struct. Crystallogr. & Cryst. Chem.* **24**, 1107 (1968).
[69] J. Hu, M. Chen, X. Fang, L. Wu. *Chem. Soc. Rev.* **40**, 5472 (2011).
[70] L. Ratke, P. W. Voorhees, In: *Growth and Coarsening: Ostwald Ripening in Material Processing*, pp. 117–118, Springer-Verlag Berlin Heidelberg NewYork, (2002).
[71] X. L. Zhao, R. Qiao, J. C. Kim, Y. S. Kang. *Cryst. Growth & Des.* **8**, 2609 (2008).
[72] V. Michael, M. Klaumünzer, H. Thiem, W. Peukert. *J. Phys. Chem. C*, **114**, 6243 (2010).
[73] D. Murnane, C. Marriott, G. P. Martin. *Cryst. Growth & Des.* **8**, 2753 (2008).
[74] H. C. Zeng. *Curr. Nanosci.* **3**, 177 (2007).
[75] J. Li, H. C. Zeng. *J. Am. Chem. Soc.* **129**, 15839, (2007).
[76] H. G. Yang, H. C. Zeng. *J. Phys. Chem. B* **108**, 3492 (2004).
[77] P. Wang, K. Yokoyama, T. Konishi, N. Nishiwaki, K. Kobiro. *J. Supercrit. Fluids* **80**, 71 (2013).
[78] K. Soga, W. Wang, R. E. Riman, J. B. Brown, K. R. Mikeska. *J. Appl. Phys.* **93**, 2946 (2003).
[79] Mole ratio of host metal oxide to dopant in the reaction mixture.
[80] We prepared two types of RE doped MARIMO NPs, since reciprocal high and low concentrations of RE on MARIMO NPs are necessary for EDX mapping and photoluminescence, respectively.
[81] J. Silver, M. I. Martinez-Rubio, T. G. Ireland, G. R. Fern, R. Withnall. *J. Phys. Chem. B* **105**, 948 (2001).
[82] P. Zhao, Y. Zhu, X. Yang, K. Fan, J. Shen, C. Li. *RSC Adv.* **2**, 10592 (2012).
[83] W. Luo, C. Fu, R. Li, Y. Liu, H. Zhu, X. Chen. *Small* **7**, 3046 (2011).
[84] X. Chen, W. Luo. *J. Nanosci. Nanotechn.* **10**, 1482 (2010).
[85] S. Jeon, P. V. Braun. *Chem. Mater.* **15**, 1256 (2003).
[86] A. Patra, C. S. Friend, R. Kapoor, P. N. Prasad. *Chem. Mater.* **15**, 3650 (2003).
[87] A. Patra, C. S. Friend, R. Kapoor, P. N. Prasad. *J. Phys. Chem. B* **106**, 1909 (2002).
[88] J. H. Pan, Z. Cai, Y. Yu, X. S. Zhao. *J. Mater. Chem.* **21**, 11430 (2011).
[89] L. Hou, P. Wang, F. Kong, H. Park, K. Kobiro, T. Ohama. *Phycol. Res.* **61**, 58 (2013).